Level structure of the neutron-rich ^{56,58,60}Cr isotopes: Single-particle and collective aspects

S. Zhu,[1] A. N. Deacon,[2] S. J. Freeman,[2] R. V. F. Janssens,[1] B. Fornal,[3] M. Honma,[4] F. R. Xu,[5] R. Broda,[3] I. R. Calderin,[6] M. P. Carpenter,[1] P. Chowdhury,[7] F. G. Kondev,[8] W. Królas,[3] T. Lauritsen,[1] S. N. Liddick,[9,10] C. J. Lister,[1] P. F. Mantica,[9,10] T. Pawłat,[3] D. Seweryniak,[1] J. F. Smith,[2] S. L. Tabor,[6] B. E. Tomlin,[9,10] B. J. Varley,[2] and J. Wrzesiński[3]

[1]*Physics Division, Argonne National Laboratory, Argonne, Illinois 60439, USA*

[2]*School of Physics and Astronomy, Schuster Laboratory, University of Manchester, Manchester M13 9PL, United Kingdom*

[3]*Institute of Nuclear Physics, Polish Academy of Sciences, PL-31342 Cracow, Poland*

[4]*Center for Mathematical Sciences, University of Aizu, Tsuruga, Ikki-machi, Aizu-Wakamatsu, Fukushima 965-8580, Japan*

[5]*Department of Technical Physics, Peking University, Beijing 100871, China*

[6]*Department of Physics, Florida State University, Tallahassee, Florida 32306, USA*

[7]*University of Massachusetts, Lowell, Massachusetts 01854, USA*

[8]*Nuclear Engineering Division, Argonne National Laboratory, Argonne, Illinois 60439, USA*

[9]*National Superconducting Cyclotron Laboratory, Michigan State University, East Lansing, Michigan 48824, USA*

[10]*Department of Chemistry, Michigan State University, East Lansing, Michigan 48824, USA*

(Received 6 September 2006; published 26 December 2006)

The structure of the ^{56,58,60}Cr nuclei was investigated at Gammasphere using both deep inelastic and fusion-evaporation reactions. As a result of this work, expanded level schemes are now available for these three neutron-rich, even-even isotopes. Experimental signatures were found for both single-particle and collective excitations whose relative importance varies with neutron number. Together with recent structural information on the odd-A ^{55,57,59}Cr neighbors, the present data highlight the changing role of the $g_{9/2}$ orbital with neutron number. Comparisons with shell-model calculations using the recently developed GXPF1A interaction and with total Routhian surface calculations are presented.

DOI: 10.1103/PhysRevC.74.064315 PACS number(s): 21.60.Cs, 23.20.Lv, 27.40.+z, 27.50.+e

I. INTRODUCTION

Over the last few years, the properties of exotic nuclei, i.e., nuclei away from the valley of stability, have been investigated extensively in both experimental and theoretical studies. The primary motivation for these studies has been the expectation that substantial modifications can occur to the intrinsic shell structure of nuclei with a sizable neutron excess [1,2]. As a result, some familiar magic numbers may no longer apply while new ones appear. The vanishing of the $N = 20$ shell gap, which occurs in the so-called island of inversion encompassing neutron-rich nuclei such as ^{30}Ne, ^{31}Na, and ^{32}Mg [3–5], is one of the best examples of such structural changes. The presence of deformed, rather than spherical, ground-state configurations is the result of the lowering of the intruder *fp* states due to strong interactions between valence protons and neutrons, between the valence neutrons themselves, and shifts in single-particle energies [6,7]. Another recent example of structural changes is the appearance of an $N = 32$ subshell closure in neutron-rich nuclei located just above the doubly magic nucleus $^{48}_{20}$Ca$_{28}$ [8,9].

The $N = 32$ subshell gap was first proposed in ^{52}Ca by Huck *et al.* [10] to explain the surprisingly large excitation energy of its first excited state, $E(2^+_1)$, as compared with the corresponding value in ^{50}Ca. Recently, studies in chromium ($Z = 24$) [8,11] and titanium ($Z = 22$) [9] isotopes found that $E(2^+_1)$ values also maximized at ^{56}Cr$_{32}$ and ^{54}Ti$_{32}$, two isotopes with $N = 32$. This subshell closure also manifests itself through the large energy gap between the lowest 6^+ level and higher spin states in ^{54}Ti, reflecting the high energy cost of promoting neutrons across this $N = 32$ gap. The recently developed GXPF1 effective interaction was found to be able to account for the $N = 32$ gap as resulting from a weakening of the $\pi 1f_{7/2}$-$\nu 1f_{5/2}$ proton-neutron monopole interaction as protons are removed from the $1f_{7/2}$ single-particle orbital (filled at $Z = 28$), combined with a significant $\nu 2p_{1/2}$-$\nu 2p_{3/2}$ spin-orbit splitting [12]. To place the above interpretation on firmer ground, the $B(E2; 0^+ \rightarrow 2^+_1)$ reduced transition probabilities were measured for the $^{52-56}$Ti even isotopes [13]. The fact that the 2^+_1 excitation energy and reduced transition probability observed in ^{54}Ti are comparable to those in ^{50}Ti confirmed that the $N = 32$ Ti isotope is as good a semimagic nucleus as its $N = 28$ counterpart and, hence, that a substantial subshell gap must occur at $N = 32$. A recent study of ^{52}Ca with a two-proton knockout reaction also confirmed the presence of the neutron subshell closure at $N = 32$ [14]. However, the absence in the Ti isotopic chain of a subshell gap at $N = 34$ [15–17], predicted by the GXPF1 interaction, has led to a modified version of the Hamiltonian, labeled as GXPF1A [18], in which five $T = 1$ matrix elements of the interaction, involving mainly the $\nu p_{1/2}$ and $\nu f_{5/2}$ single-particle orbitals, have been readjusted. The GXPF1A calculations provide a satisfactory description of all the known levels in the even Ti nuclei, including those above the 6^+ level in ^{54}Ti which involve neutron excitations across the $N = 32$ shell closure. They also describe the odd Ti nuclei satisfactorily [19].

As indicated by the systematics of the 2^+_1 energies of the even-even Cr isotopes from $N = 28$ to $N = 34$, the effect of the $N = 32$ shell gap is less pronounced in this isotopic chain. This is expected since two additional protons occupy the $f_{7/2}$ shell, and the $\pi 1f_{7/2}$-$\nu 1f_{5/2}$ proton-neutron monopole

interaction is correspondingly stronger. Nevertheless, results from a recent study of the $B(E2; 0^+ \rightarrow 2_1^+)$ transition probabilities indicate that the collectivity of the 2_1^+ state in ^{56}Cr (with $N = 32$) is significantly lower than that in the neighboring $N = 30$ and $N = 34$ isotopes, ^{54}Cr and ^{58}Cr, and is similar to that of $N = 28$, ^{52}Cr [20].

Another experimental observation is that for neutron numbers above $N = 32$, the 2_1^+ energy starts to drop considerably: from 1007 keV in ^{56}Cr [11] to 880 in ^{58}Cr [8], 645 in ^{60}Cr, and 446 in ^{62}Cr [21]. This trend of decreasing 2_1^+ energies may possibly be due to a small neutron gap at $N = 40$, which will facilitate excitations to the $\nu g_{9/2}$ intruder orbital. Recent detailed studies of odd, neutron-rich Cr isotopes reveal that the yrast $9/2^+$ state, which is associated with this $\nu g_{9/2}$ intruder orbital, decreases in excitation energy with increasing neutron number: from 2087 keV in ^{55}Cr to 1507 in ^{57}Cr and abruptly down to 503 in ^{59}Cr. In ^{55,57}Cr, decoupled rotational bands built on the $\nu g_{9/2}$ state have been reported [11,22], and these bands provide strong experimental evidence for the shape-driving potential of this intruder level, in these specific cases toward substantial prolate deformation. On the other hand, the long-lived $9/2^+$ isomeric state observed in ^{59}Cr appears consistent with an oblate or spherical core [23]. In any event, the evidence available thus far indicates an increasing involvement of the $\nu g_{9/2}$ orbital when compared to the Ti isotopes.

The observation of high-spin states in the even-even ^{56,58,60}Cr isotopes is important because it provides information about the evolution of single-particle excitations with neutron number and excitation energy, as well as about the possible onset of collectivity for neutron numbers $N \geqslant 32$. Specifically, in view of the observations in the odd Cr isotopes discussed above, the role of the $\nu g_{9/2}$ intruder state in establishing the nuclear shape needs to be documented. Also, this orbital can potentially have an impact on the presence or absence of a shell gap at $N = 40$, so tracing its role as a function of neutron number becomes particularly relevant.

The level structure of ^{56}Cr has been studied up to a spin of 13 and an excitation energy of 8767 keV in Ref. [11]. However, no negative-parity states were observed conclusively in this work. In the heavier Cr isotopes ^{58}Cr and ^{60}Cr, the first 2^+ level has been identified through β decay following projectile fragmentation [21,24]. A level scheme of ^{58}Cr has recently been proposed from a PRISMA + CLARA experiment [25] carried out at Legnaro. As this measurement suffered from low $\gamma\gamma$ coincidence rates, the placement of transitions above spin 6 in the proposed level scheme is not well established. Indeed, as will be shown here, the proposed $8^+ \rightarrow 6^+$ assignment in the level scheme of Ref. [25] is incorrect, a finding leading one to question the conclusions drawn in this work about possible evidence for a shape phase transition and a dynamical symmetry in ^{58}Cr. Preliminary results on ^{60}Cr have been reported previously in Ref. [26].

A number of experiments have demonstrated that the yrast states of hard-to-reach neutron-rich nuclei can be populated in deep inelastic processes at beam energies 15%–25% above the Coulomb barrier [27–29]. These complex reactions are also able to populate relatively high angular-momentum states, thus allowing experimental access to high-spin structures in regions inaccessible with conventional heavy-ion-induced, fusion-evaporation reactions. In the collisions between a ^{48}Ca beam and a ^{238}U or ^{208}Pb target, because of the general tendency toward N/Z equilibration of the dinuclear systems, the production of nuclei with a large neutron excess in the vicinity of ^{48}Ca is favored. Another approach to reach neutron-rich nuclei is to use neutron-rich, long-lived radioactive targets, such as ^{14}C, in combination with ^{48}Ca projectiles to produce neutron-rich compound nuclei. Neutron-rich residues, such as ^{60}Cr, can be studied via the two-proton evaporation process which occurs with a small cross section. Both types of reactions have been used here.

In this work, the high-spin states in the even-even ^{56,58,60}Cr nuclei have been investigated. The yrast and near-yrast level structures in these nuclei have been identified. They are discussed in terms of the shape-driving impact of the $\nu g_{9/2}$ orbital. Comparisons with the results of shell-model calculations with the GXPF1A Hamiltonian interaction are also discussed.

II. EXPERIMENTS

Three separate experiments using two different types of reactions were carried out with ^{48}Ca beams delivered by the Argonne Tandem-Linac Accelerator System (ATLAS) at Argonne National Laboratory. During the first run, a 305-MeV ^{48}Ca beam bombarded a 50-mg/cm^2-thick ^{208}Pb target. This beam energy is roughly 20% above the Coulomb barrier at midtarget. The beam was pulsed with a 410-ns repetition rate, each beam pulse being $\sim$0.3 ns wide. Gammasphere (GS) [30], with 101 Compton-suppressed high-purity Ge detectors, was used to collect events with three or more γ rays in coincidence. A total of 8.1×10^8 three- and higher-fold events were collected with energy and timing information for all suppressed Ge detectors firing within 800 ns of the triggering signal being recorded. The data were sorted into two-dimensional (E_γ-E_γ matrices) and three-dimensional (E_γ-E_γ-E_γ cubes) histograms under various timing conditions. The prompt $\gamma\gamma\gamma$ cube was incremented for γ rays observed within $\pm$20 ns of the beam burst, while in the delayed $\gamma\gamma\gamma$ cube, the γ-ray transitions were required to occur in an interval of $\sim$40 to $\sim$350 ns after the beam pulse, but within $\sim$40 ns of each other. In this way, events associated with isomeric deexcitation or β decay could be isolated and identified.

One of the advantages of using a ^{208}Pb target is the ability to assign newly found γ rays to specific nuclei through cross-coincidence relationships between binary reaction products, as demonstrated in Refs. [9,19]. The nuclei ^{56}Cr and ^{58}Cr could be investigated in this way by placing coincidence gates on known transitions in Pt nuclei. However, the extension of the investigation toward Cr isotopes with a larger neutron excess, such as $N = 36$ ^{60}Cr, required the use of a ^{238}U target with a more favorable neutron-to-proton ratio ($N/Z = 1.59$) than in ^{208}Pb ($N/Z = 1.54$). Therefore, a second measurement was performed with a 330-MeV ^{48}Ca beam and a 50-mg/cm^2 ^{238}U target. The beam was pulsed in the same manner as in the earlier experiment, and 2.3×10^9 three- and higher-fold events were collected with GS under the same

trigger conditions. Because, in this second measurement, the target-like products mostly undergo fission, an identification based on cross-coincidence relationships between transitions in reaction partners proved difficult and often impossible. Transitions in neutron-rich, projectile-like nuclei identified by other means have to be used as starting points for more detailed investigations of the associated level structures. Because ^{56}Cr has been studied in β decay [8] and in-beam γ-ray spectroscopy following fusion-evaporation [11], it could be used to assess the statistical accuracy of the ^{48}Ca+^{238}U data set. However, in the quest for ^{60}Cr, information obtained by other means was needed as a starting point.

Another approach used here for producing neutron-rich Cr isotopes involves the fusion of ^{48}Ca projectiles with a ^{14}C radioactive target. The 130-MeV beam energy was selected to optimize the weak, two-proton evaporation channel which produces ^{60}Cr. This beam energy turns out to be favorable also for the study of ^{56,57}Cr through the $\alpha 2n$ and αn evaporation channels, respectively. The ^{14}C target was isotopically enriched at a level of about 90% and had an approximate thickness of 100 μg/cm^2. Prompt γ rays were detected with GS consisting of 100 Compton-suppressed detectors in this instance. Reaction products recoiling from the target were passed through the Argonne Fragment Mass Analyzer (FMA) [31] and were dispersed at the focal plane of this instrument according to their mass-to-charge (A/Q) ratio. The FMA was tuned to transport ions with charge state 17^+ and mass 60 to the middle of its focal plane, where a parallel-grid avalanche counter (PGAC) was used to measure the horizontal and vertical positions of the recoils and to generate timing signals. A segmented ion chamber, located behind the focal plane, registered the energy-loss characteristics of the recoils. The data acquisition was triggered by an event corresponding to the arrival of an ion at the focal plane in coincidence with the detection of at least one γ ray in Gammasphere. Data were recorded for 128 hours with a beam current of approximately 5 pnA and a total of 3×10^8 recoil-γ events were stored on magnetic tape.

The techniques employed in the identification of events corresponding to ^{60}Cr were similar to those used in previous studies of ^{57,59}Cr [22,23]. In order to identify γ rays from ^{60}Cr in a background of $>10^5$ times more intense transitions in residues from the $3n$ and $4n$ evaporation channels, it was essential to require optimized and exclusive correlations between evaporation residues and the emitted γ rays. The combination of the total ion energy, E, and the time of flight through the FMA, T, in the form of the product ET^2 is proportional to the mass of the ion. This was used to help resolve charge state ambiguities, and the resolution in such a measurement is sufficient to separate the mass-to-charge $A/Q = 60/17$ ions from the $A/Q = 56/16$ group. The atomic number of the recoiling ions could be easily deduced from the energy-loss characteristics of the ions in the ion chamber filled with isobutane gas. This detector was segmented and had three anodes which recorded the energy losses separately (see Ref. [23] for further details).

The spin and parity quantum numbers of the levels in the three Cr isotopes were deduced, when allowed by the available statistics, from either an angular correlation analysis in the ^{48}Ca+^{238}U experiment or an angular distribution analysis in the ^{48}Ca+^{14}C case. In addition, considerations based on the fact that the reactions feed yrast states preferentially and/or on comparisons with shell-model calculations were also used. The products of deep-inelastic reactions have no, or very little, alignment. Therefore, the analysis of $\gamma\gamma$ angular correlations for selected pairs of transitions is one suitable way to assign spin and parity quantum numbers to observed states. As described in detail in Ref. [19], two coincidence matrices were constructed. All pairs of γ rays measured in detectors with angles relative to each other between 20° and 37° were placed in one coincidence matrix, while those pairs with angles between 79° and 90° were placed into another. The intensity ratio from each matrix at a point (E_{γ_1}, E_{γ_2}) reflects the angular correlation between transitions γ_1 and γ_2 at the average angles of 28° and 85°. For a cascade of two stretched transitions, the ratio is unique; but for mixed transitions, it can vary considerably and depends on the value of the mixing ratio. In practice, in order to avoid ambiguities in the spin assignments as much as possible, at least one known stretched transition was included in every correlation analysis.

The multipolarity assignments of the states observed in fusion-evaporation residues were based primarily on angular distributions, in combination with the DCO (Directional Correlation of Oriented nuclei) ratios, as the compound nuclei are formed in an "aligned" state, i.e., the nuclear spin is located in a plane perpendicular to the beam axis. Angular distributions $W(\theta)$ were fitted with the formula

$$W(\theta) = A_0[1 + a_2 P_2(\cos\theta) + a_4 P_4(\cos\theta)], \qquad (1)$$

where P_2 and P_4 are Legendre polynomials. DCO ratios were extracted from matrices in which the energy of γ rays measured in the detector rings close to 90° (79.1°, 80.8°, 90.0°, 99.3°, and 100.8°) were incremented against those close to 0° and 180° (17.3°, 31.7°, 37.3°, 142.6°, 148.3°, and 162.7°) and were defined as

$$R_{\mathrm{DCO}} = \frac{I^{\gamma_2}_{0/180}(\mathrm{Gate}^{\gamma_1}_{90})}{I^{\gamma_2}_{90}(\mathrm{Gate}^{\gamma_1}_{0/180})}. \qquad (2)$$

Typical R_{DCO} values for transitions of dipole character are $R_{\mathrm{DCO}} \sim 0.5$–$0.6$, while quadrupole transitions group around $R_{\mathrm{DCO}} \sim 1.0$.

III. RESULTS

A. ^{56}Cr

The ^{56}Cr level scheme obtained from the three measurements with Gammasphere is given in Fig. 1. As a semimagic nucleus with $N = 32$, ^{56}Cr has been studied previously through β decay of ^{56}V produced by intermediate-energy projectile fragmentation [24,32] and with prompt spectroscopy following fusion-evaporation reactions [11,33]. The information from these studies served as a starting point for the analysis of the complex data from the ^{48}Ca + ^{208}Pb and ^{48}Ca + ^{238}U measurements. In fact, for ^{56}Cr, the data set from the latter reaction proved to be of higher statistical significance, and it was used most extensively.

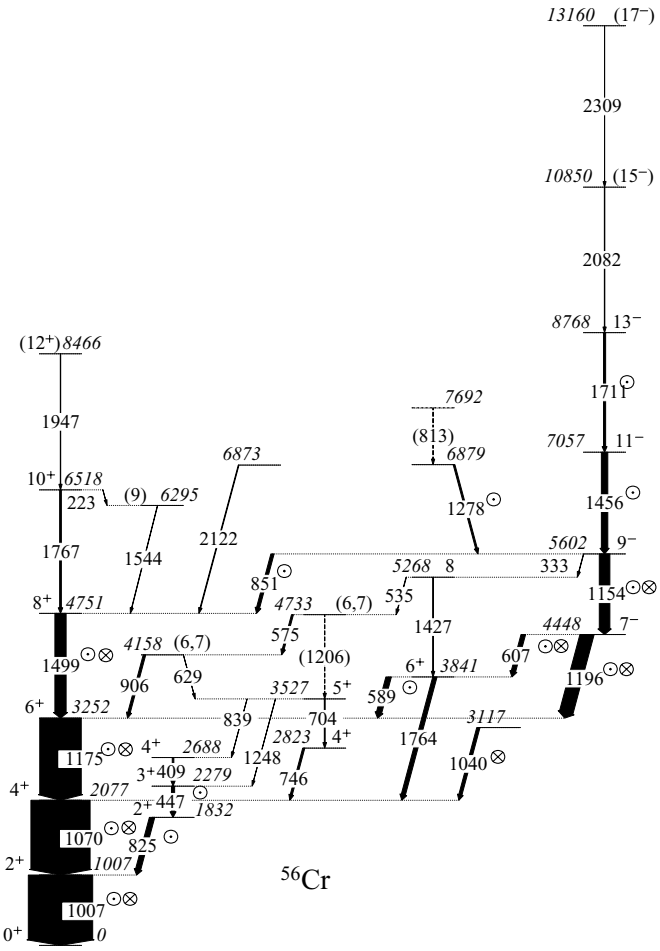

FIG. 1. Level scheme for ^{56}Cr derived in the present work. States are labeled by spin-parity and excitation energy to the nearest keV. Electromagnetic transitions are indicated by arrows whose widths indicate their intensity and are labeled by transition energy in keV. Transitions observed in deep inelastic reactions are indicated with ⊗ symbols; those from Ref. [34] are given by the ⊙ symbols. All other transitions result from the analysis of the ^{14}C(^{48}Ca, $\alpha 2n$) reaction. See text for details.

In the present work, only eight ^{56}Cr transitions were observed through deep inelastic reactions; they are indicated in Fig. 1 with ⊗ symbols. This is six fewer transitions than were observed in Ref. [11] from a study of a $p2n$ fusion-evaporation reaction carried out with the Yale YRASTBall array [34] consisting of 24 Compton-suppressed Ge detectors (the transitions seen in the latter work are indicated in Fig. 1 by the ⊙ symbols). The only new transition based on coincidence data from the deep inelastic reactions is a 1040-keV γ ray feeding the 2077-keV, 4^+ yrast state. This transition was, however, too weak to obtain angular correlation data of sufficient accuracy to provide spin and parity quantum numbers for the 3117-keV level. From the ^{48}Ca + ^{238}U data, the highest observed transition is the 1154-keV γ ray linking the 5602- and 4448-keV states. The deexcitation from this level splits into two branches associated with the 607- and 1196-keV lines. Only the sequence associated with the second γ ray could be followed entirely, as the weaker path

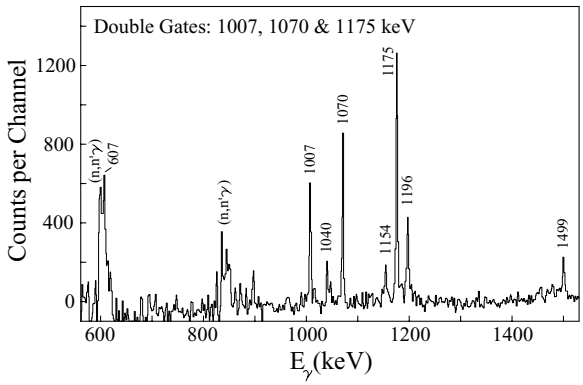

FIG. 2. Coincidence spectrum in ^{56}Cr from the ^{48}Ca + ^{238}U reaction obtained by placing double coincidence gates on pair-wise combinations of the 1007-, 1070-, and 1175-keV transitions. Peaks are labeled by transition energy in keV.

involving the 607-keV transition could not be traced below the 3841-keV state because of contamination of the 589- and 1764-keV lines. The multipolarities of the 1007-, 1070-, 1175-, and 1196-keV transitions were determined from the angular correlation analysis. The relevant coefficient for the 1007–1070 keV pair of γ rays is 1.16(3), while those for the 1070–1175 and 1175–1196 keV pairs are 1.29(4) and 0.87(9), respectively. These results are consistent with the assignments of Ref. [11] associating these four transitions with a $7^- \rightarrow 6^+ \rightarrow 4^+ \rightarrow 2^+ \rightarrow 0^+$ cascade. The quality of the data is illustrated in Fig. 2 with a double-gated coincidence spectrum in which the eight γ rays of interest are clearly visible. The absence of transitions from higher levels is probably due, at least in part, to the fact that fast transitions (with lifetimes typically <1 ps) are undetectable in thick target data because of Doppler broadening. Differences in feeding patterns are likely to be another contributing factor.

In the GS+FMA experiment where ^{56}Cr was produced through the ^{14}C(^{48}Ca, $\alpha 2n$) reaction channel, the optimum energy resolution in the γ-ray spectra was achieved by performing the Doppler shift correction on an event-by-event basis using the time of flight between the PGAC and the rf signal from the accelerator. The procedure is described in detail in Ref. [35], and the quality of the data is illustrated by the coincidence spectrum of Fig. 3. As can be seen in the full level scheme of Fig. 1, a total of 32 transitions were observed with this reaction, the main cascades of positive and negative parity were extended beyond the work of Ref. [11], and numerous non-yrast levels were identified as well.

Table I summarizes the available information on the intensity and multipolarity of the various γ rays from the fusion reaction, with the 1040-keV transition mentioned above added for completeness. Spin and parity assignments are proposed on the basis of the measured angular distributions whenever possible, with further support from the DCO ratios. The latter were obtained from spectra gated by the 1007-keV $2^+ \rightarrow 0^+$ transition. However, it should be noted that DCO ratios obtained with coincidence gates on other strong transitions (not listed in Table I) provided additional support for the assignments.

TABLE I. Level and γ-ray transitions in the deduced level scheme of ^{56}Cr. Level (E_{level}) and γ-ray energies (E_γ) are given in keV; intensities (I_γ) are normalized to 100. The a_2 and a_4 coefficients are defined in Eq. (1) and associated with the angular distribution fits.

E_{level} (keV)	J^π	E_γ (keV)	I_γ	a_2	a_4	DCO
1007	2^+	1006.9(1)	100.0(3)	0.102(15)	−0.067(19)	
1832	2^+	824.8(1)	8.1(4)			0.8(3)
2077	4^+	1070.0(1)	92.0(3)	0.159(15)	−0.080(20)	1.1(1)
2279	3^+	446.8(1)	4.94(20)	−0.231(45)		0.7(2)
2688	4^+	409.4(1)	2.44(10)	−0.365(61)		0.9(4)
2823	4^+	746.1(1)	3.17(19)	0.221(73)	0.034(98)	0.5(2)
3117[a]		1039.9(5)	5.4(5)			
3252	6^+	1175.1(1)	64.5(20)	0.237(18)	−0.138(23)	1.1(1)
3527	5^+	704.0(10)	1.31(9)	−0.490(96)		0.5(3)
		839.0(10)	0.73(5)			0.3(3)
		1248.4(10)	0.58(7)			
3841	6^+	589.2(1)	8.3(3)	−0.029(38)	−0.273(51)	1.1(3)
		1763.8(2)	6.5(3)	0.168(44)	−0.076(58)	
4158	(6,7)	629.0(1)	0.15(4)			
		905.7(1)	3.78(19)			
4448	7^-	606.5(1)	6.90(24)	−0.566(44)		0.6(2)
		1196.2(1)	21.3(7)	−0.287(26)		0.5(1)
4733	(6,7)	574.9(1)	2.92(13)	−0.133(55)	−0.781(73)	1.0(4)
		1205.5(10)	0.62(8)			
4751	8^+	1499.2(1)	17.4(6)	0.280(35)	−0.122(47)	1.2(3)
5268	8	534.9(4)	0.62(5)			
		1426.9(6)	1.00(11)			0.8(6)
5602	9^-	332.7(2)	0.46(4)	−0.266(81)		0.6(5)
		850.6(1)	4.85(19)			0.6(2)
		1153.6(1)	16.4(5)	0.271(29)	−0.226(41)	1.5(3)
6295	(9)	1544.3(10)	0.50(12)			
6518	10^+	222.9(10)	0.16(3)			
		1767.3(4)	2.67(21)	0.168(44)	−0.076(58)	
6873		2121.9(1)	1.05(15)			
6879		1277.5(2)	2.62(14)			
7057	11^-	1455.7(1)	10.0(4)	0.323(40)	−0.133(53)	1.3(3)
7692		812.9(1)	0.68(7)			
8466	(12^+)	1947.2(16)	0.58(12)			
8768	13^-	1710.9(2)	3.26(16)	0.402(79)	−0.004(109)	
10850	(15^-)	2081.9(3)	0.70(12)			
13160	(17^-)	2309.4(10)	0.22(12)			

[a]Observed in the ^{48}Ca + ^{238}U data only.

The yrast sequence of positive parity was extended up to the tentative 12^+ level at 8466 keV through the addition of the 1767- and 1947-keV transitions. These are in coincidence with the 1499 → 1175 → 1070 → 1007 keV cascade. The angular distribution of the 1767-keV line is consistent with a transition of stretched-$E2$ character. Unfortunately, the 1947-keV γ ray is too weak to provide angular distribution information, and the 12^+ quantum numbers of the 8466-keV state are tentatively proposed solely on the basis of the fact that this transition represents the natural extension of the positive-parity sequence.

Compared to the work of Ref. [11], the ordering of some odd-spin levels has been altered and a "rotational-like" sequence of five transitions is proposed on the basis of the measured intensities (Fig. 1). As discussed in detail below, this arrangement in a cascade is confirmed in part by a striking similarity with the $g_{9/2}$-based rotational structures of ^{55,57}Cr [11,22]. The deexcitation of the 4448-keV state at the bottom of this sequence has been revised with respect to the earlier work [11] because of the newly observed 1764-keV line, which is in coincidence with the 1070- and 607-keV transitions, but is absent in the spectra gated on both the 1175- and 589-keV γ rays. These observations, together with the fact that the 1764-keV energy equals that of the sum of the coincident 589- and 1175-keV lines, reverse the order of the 589- and 607-keV transitions and move the intermediate state from the 3860-keV energy proposed in Ref. [11] to the 3841-keV energy of Fig. 1. This change is further justified by coincidence relationships between transitions feeding and deexciting a number of weakly-populated nearby states at 3527, 4158, 4733,

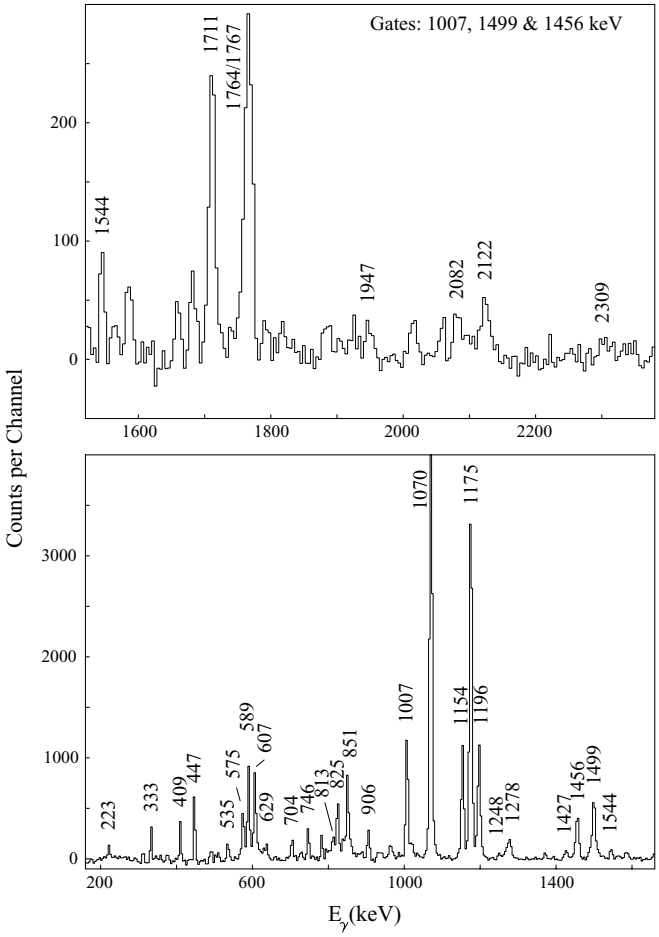

FIG. 3. Representative coincidence spectrum in ^{56}Cr from the ^{48}Ca + ^{14}C measurement, obtained by summing gates placed on the 1007-, 1499-, and 1456-keV transitions. Peaks are labeled by the transition energy in keV.

and 5268 keV. The spin and parity of the 4448-keV level is established as 7^- by its main deexcitation branch through the 1196-keV γ ray with angular distribution and DCO coefficients consistent with a transition of dipole character, combined with the observations for the parallel decay pathway. In the latter, a 607-keV transition is of stretched-dipole character [negative a_2 coefficient, DCO ratio of 0.6(2)] and establishes the 3841-keV level as 6^+. These quantum numbers are in turn consistent with the measured anisotropy of the 589-keV line, which is characteristic of a $\Delta I = 0$ transition with a mixing ratio of $\delta \simeq +1.2$. The 6^+ assignment to the 3841-keV state also agrees with the likely $E2$ character of the 1764-keV line, although the latter is poorly resolved from the 1767-keV $10^+ \rightarrow 8^+$ γ ray, and the anisotropy coefficients quoted in Table I are those measured for the combined intensity of the two transitions. The stretched-$E2$ character of the 1154-, 1456-, and 1711-keV transitions leads to the 9^-, 11^-, and 13^- assignments for the 5602-, 7057-, and 8768-keV levels of the negative-parity band. The similarity with the structures in the odd-Cr neighbors mentioned above and the fact that the 2082- and 2309-keV lines appear to represent the natural extension of the sequence justify the tentative assignment of $I^\pi = 15^-$ and 17^- to the higher lying 10850- and 13160-keV states. It is worth noting that the 9^- assignment to the 5602-keV level is supported further by the measured DCO ratio of the 851-keV line. This state also decays through another pathway defining another spin 8 level at 5268 keV with the 333-keV γ ray of dipole character. This spin 8 state then decays via transitions of 1427 and 535 keV. Because of weak statistics and likely contamination, no meaningful angular distribution or DCO ratio was obtained for either of these transitions.

Angular distributions were difficult to obtain for the unresolved multiplet of transitions with energies of 813, 825, 839, and 851 keV. The 825-keV transition feeds into the 2_1^+ state, and although its DCO ratio is inconclusive, yrast feeding arguments suggest that the spin of the 1832-keV level is unlikely to be higher than $3\hbar$. Above this line, the angular distributions for the 409- and 447-keV γ rays are consistent with a stretched-dipole nature, giving spins of at most $4\hbar$ and $5\hbar$ for the 2279- and 2688-keV states, respectively. Further restrictions on the possible spin values are provided by the two alternative decay paths out of the 3527-keV state via the 839–1248 and 704–746 keV pairs. The 746-keV angular distribution is somewhat complicated by contaminants; it is clearly characterized by a positive a_2 coefficient, although a statistically significant a_4 value could not be extracted. This information, along with the DCO ratio of 0.5(2), is reproduced by a $\Delta I = 0$ transition with a predominant $E2$ component. The unambiguous stretched-dipole nature of the 704-keV line then fixes the spin of the 3527-keV state as $I = 5$. The decay of this level through the 839-keV γ ray with a DCO ratio of 0.3(3) gives likely spins of 4, 3, and 2 to the 2688-, 2279-, and 1832-keV states. These values are consistent with the firm assignment of 2^+ to the 1832-keV level in Refs. [11] and [24].

Spins of the states at 4158 and 4733 keV are suggested on the basis of angular momentum selection rules applied to the interconnections with known levels. The angular distribution of the 575-keV transition between this pair of states appears to suggest a folded transition which fits with the proposed spin values.

B. ^{58}Cr

Present knowledge about the structure of ^{58}Cr comes from recent β-decay measurements of ^{58}V produced in projectile fragmentation [8,24] where an 880-keV γ ray was proposed as the $2^+ \rightarrow 0^+$ ground-state transition, and five additional weaker transitions were reported as well, but were not placed in a level scheme. Recently, using the ^{64}Ni + ^{238}U reaction at 400 MeV, Marginean *et al.* [25] observed four transitions with energies 1371, 1280, 1057, and 880 keV and proposed that these correspond to the $(8^+) \rightarrow (6^+) \rightarrow 4^+ \rightarrow 2^+ \rightarrow 0^+$ yrast cascade.

The cross-coincidence relationships have been analyzed between the 881-keV ^{58}Cr γ ray and transitions in Pt isotopes, the complementary products from the ^{48}Ca+^{208}Pb reaction. Because of neutron evaporation, ^{58}Cr is associated with several Pt partners, including ^{194}Pt and ^{192}Pt. Spectra with double coincidence gates placed on the 881-keV line and $2^+ \rightarrow 0^+$ transitions in ^{194,192}Pt are presented in Figs. 4(a) and 4(b).

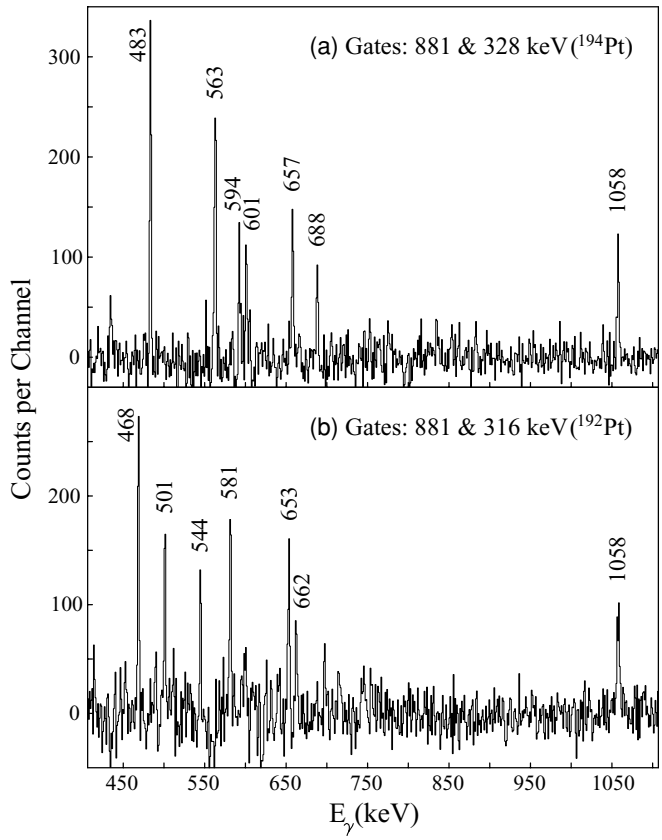

FIG. 4. Representative cross-coincidence γ-ray spectra from the ^{48}Ca + ^{208}Pb reaction double gated by the 881-keV, $2^+ \rightarrow 0^+$ transition in ^{58}Cr and (a) the 328-keV, $2^+ \rightarrow 0^+$ transition in ^{194}Pt and (b) the 316-keV, $2^+ \rightarrow 0^+$ transition in ^{192}Pt.

While most lines in the two spectra belong to the Pt nuclei, a 1058-keV γ ray is clearly present as well. In fact, it is the second strongest γ ray in the ^{58}Cr nucleus, not only in deep inelastic reactions, but also in β decay [24]. Furthermore, as shown in the inset of Fig. 6, the measured angular correlation for the 881–1058 keV pair strongly favors an $E2$ character for the two transitions. Hence, the available experimental evidence agrees with a $4^+ \rightarrow 2^+ \rightarrow 0^+$ cascade, as proposed in Ref. [25].

Just as in the case of ^{56}Cr, the ^{48}Ca + ^{238}U data proved to be most suitable for the construction of the extended level scheme of ^{58}Cr (Fig. 5). Table II summarizes all the information available for the various levels and transitions. Two parallel branches have been uncovered above the 4^+ state at 1939 keV; this is illustrated by the coincidence spectra of Fig. 6. The two strongest lines, besides the 1058- and 881-keV transitions, are the 1373- and 1281-keV γ rays, which are essentially equal in intensity and are both in coincidence with the $4^+ \rightarrow 2^+ \rightarrow 0^+$ cascade, but not with each other. In addition, the angular correlation data (see Table II) clearly show that while the 1281-keV line is of $E2$ character, the 1373-keV γ ray is not. Rather, it is a dipole transition with a small mixing ratio ($\sim$0.05), if any. In addition, the comparable intensities of the 1373- and 1281-keV transitions suggest that an $M1/E2$ character is unlikely for the former line and, as a result, a $5^{(-)}$ state is proposed at 3311 keV. Three additional levels could be placed on top of the 3311-keV $5^{(-)}$ state: six weak lines firmly establish levels at 3715, 4185, and 4670 keV, for which the proposed spin and parity quantum numbers are tentative and guided mostly by the measured anisotropies of the 404- and 1373-keV γ rays, as well as by considerations based on angular momentum selection rules for the many interconnecting transitions. On the other hand, just as in the work of Ref. [25], the 6^+ state is located at 3219 keV. However, the next transition in the positive-parity sequence appears to be the weak 1460-keV γ ray, thereby placing the next state, with a tentative spin-parity assignment of 8^+, at 4680 rather than 4588 keV, as proposed in Ref. [25]. In Fig. 6, the broadened line shape of the 1460-keV γ ray is notable, suggesting that

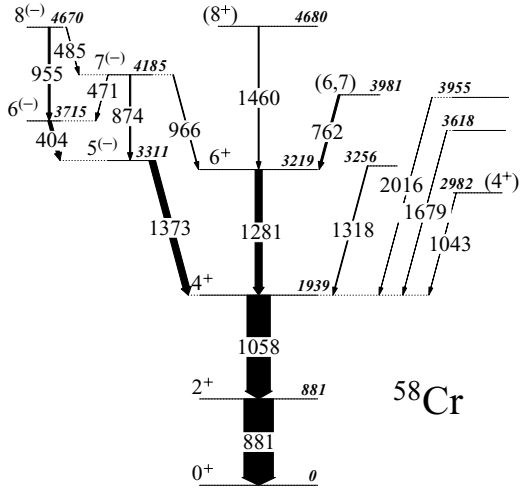

FIG. 5. Proposed level scheme for ^{58}Cr derived from the ^{48}Ca + ^{238}U experiment.

TABLE II. Levels with spin-parity assignments and γ rays identified in ^{58}Cr, including intensities, placements, and relevant ratios from the angular correlation analysis.

E_{level} (keV)	J^π	E_γ (keV)	I_γ	R_{ac}	$E_{\text{gate}\gamma}$ (keV)
881	2^+	880.7(2)	100(3)	1.21(3)	1057.9(3)
1939	4^+	1057.9(3)	79(4)	1.21(3)	880.7(2)
2982[a]	(4^+)	1043.2(2)	0.1(1)		
3219	6^+	1280.5(3)	24(2)	1.24(6)	1057.9(3)
3256		1317.5(3)	3(1)		
3311	$5^{(-)}$	1372.5(3)	23(1)	0.88(4)	1057.9(3)
3618[a]		1679.1(3)	0.1(1)		
3715	$6^{(-)}$	404.2(1)	11(2)	0.75(3)	1057.9(3)
3955[a]		2016.1(3)	0.1(1)		
3981	(7^+)	761.9(2)	7(2)	0.94(8)	1280.5(3)
4185	$7^{(-)}$	966.1(2)	3(1)		
		873.9(3)	4(1)		
		470.6(2)	1.5(5)		
4670	$8^{(-)}$	955.1(3)	7(1)		
		484.8(2)	1.0(5)		
4680	(8^+)	1460.4(3)	3(1)		

[a]Observed only with beam off.

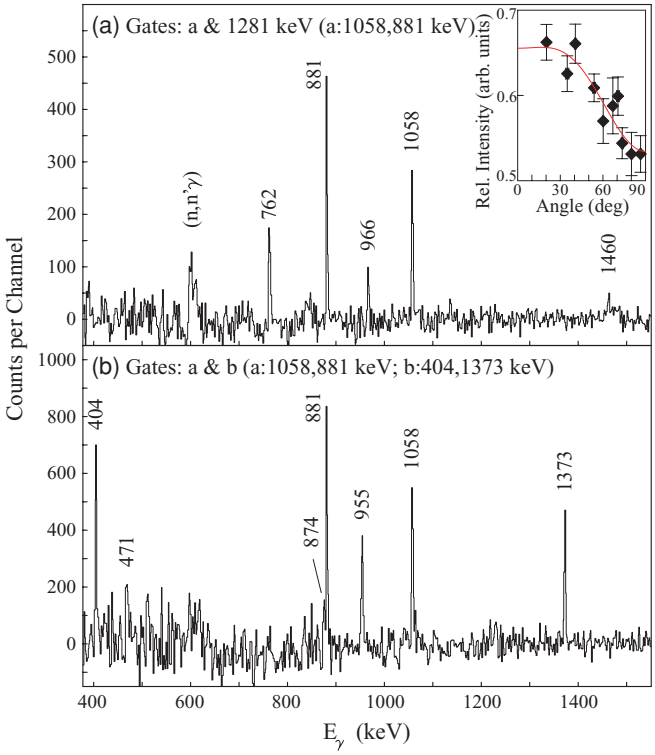

FIG. 6. (Color online) Representative coincidence γ-ray spectra double gated by the specified transitions in ^{58}Cr from the ^{48}Ca + ^{238}U reaction. Insert in upper panel shows angular correlation for the 881- and 1058-keV transitions with a_{22} and a_{44} coefficients fitted as 0.16(6) and −0.06(4).

the lifetime of the 8^+ level is comparable to the stopping time of ^{58}Cr in the target (∼3 ps).

Finally, on the right-hand side of the level scheme of Fig. 5, four additional states are reported. The 3256-keV level is established through a weak 1318-keV transition observed in the spectrum with double coincidence gates on the 881- and 1058-keV lines (not shown). The transition is too weak to derive a meaningful angular correlation, and no spin and parity quantum numbers are proposed as a result. The three other states at 2982, 3618, and 3955 keV were all observed following a careful analysis of the data taken between the beam bursts (410 ns). The coincidence spectrum double gated on the 881- and 1058-keV delayed transitions (Fig. 7) shows three γ rays, one of which (1043 keV) has been observed in β decay [24]. The other two lines at 1679 and 2016 keV were not seen in this β-decay study, but are clearly visible in Fig. 7. Their observation then suggests the presence of a weakly-fed, long-lived state in ^{58}Cr for which no further information could be derived because of the weak intensities involved.

C. ^{60}Cr

Prior to the present work, little was known about the excited states of ^{60}Cr, except for the 2_1^+ to ground-state transition proposed by Sorlin *et al.* [21] from a β-decay study of ^{60}V. Here, the ^{14}C(^{48}Ca, $2p$) reaction, carried out with Gammasphere and the FMA, provided the first delineation

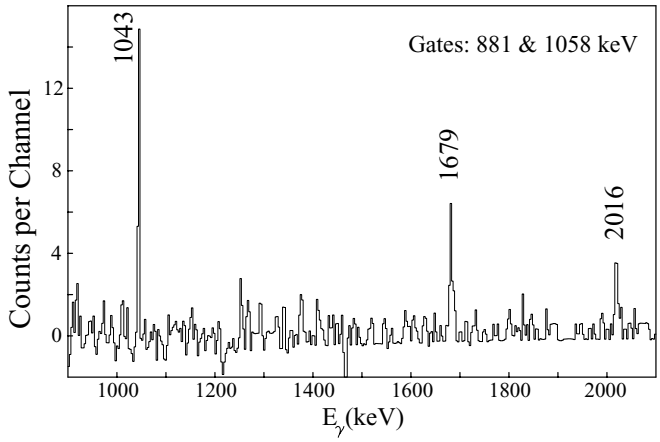

FIG. 7. Out-of-beam coincidence spectrum for ^{58}Cr.

of the yrast line on the basis of the recorded recoil-γ and recoil-$\gamma\gamma$ data, with an estimated cross section of only a few microbarns. As stated above, the combination of the total ion energy E and the time of flight through the FMA, T, in the form ET^2 is proportional to the mass of the ion; this relationship was used to help resolve charge-state ambiguities, as seen in Fig. 8(a), where the resolution is sufficient to separate the $A/Q = 60/17$ ions from the $A/Q = 56/16$ group. Figure 8(b) illustrates the fact that the atomic number of the recoiling ion is easily deduced from the energy-loss characteristics of the ions in the ion chamber. The Cr band in this plot has two distinct lobes. These occur as the Cr yield is dominated by channels involving evaporation of an α particle, and the acceptance of the FMA restricts the Cr evaporation products to tight cones

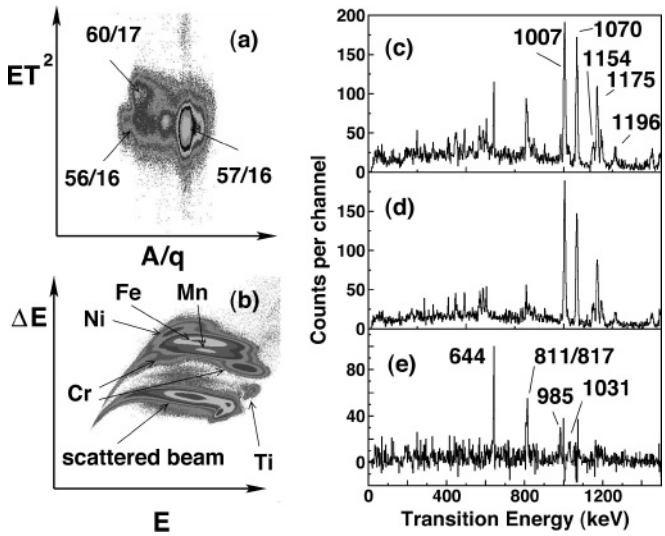

FIG. 8. Two-dimensional plots for ion identifications: (a) ET^2 vs A/Q of ions with various ion groups labeled by A/Q; (b) ΔE vs E; all axes are in arbitrary units. Coincident γ-ray spectra under various conditions: (c) spectrum gated by $A/Q = 60/17$ and $Z = 24$ with transitions in ^{56}Cr labeled by the transition energy to the nearest keV; (d) similar spectrum, but gated on $A/Q = 56/16$ and $Z = 24$; (e) normalized subtraction of (d) and (c); see text for further details.

corresponding to α evaporation near 0°and180° with respect to the beam direction, leading to high- and low-energy Cr ions. Coincidence conditions were placed on the groups in Figs. 8(a) and 8(b) corresponding to the selection of $A/Q = 60/17$ and $Z = 24$ ions: the resulting γ-ray spectra are given in Figs. 8(c)–8(e). Panel (c) is the raw spectrum with these gates applied. It is clear that the tail of the considerably more intense $A/Q = 56/16$, $Z = 24$ ion group leaks into this gate. Moreover, the peaks arising from this channel have a noticeably larger width arising from a larger spread in recoil velocities associated with α-particle evaporation. Other lines are present which, without the ET^2 selection, would be obscured by the ^{56}Cr events. Figure 8(d) provides the spectrum gated on the tail of the $A/Q = 56/16$, $Z = 24$ group, away from the $A = 60$ peak, clearly identifying the leak-through ^{56}Cr peaks. Figure 8(e) was then obtained through a normalized subtraction of the two spectra of Figs. 8(c) and 8(d), and this last panel of the figure therefore contains the lines assigned as transitions in ^{60}Cr. A total of six γ transitions with energies 644, 817, 985, 1031, 1175, and 811 keV has been identified. From $\gamma\gamma$ coincidence relations (see Fig. 9) and intensity arguments, the level scheme of ^{60}Cr is proposed as shown in Fig. 10 and reported in Table III. Thus, the first four transitions listed above form the yrast cascade. The 1175- and 811-keV lines are in coincidence only with the $2^+ \rightarrow 0^+$ transition (Fig. 9), justifying the placement in Fig. 10. Probable spin values of (3, 4) and (5, 6) are proposed for the ensuing levels at 1819 and 2630 keV based primarily on intensity and yrast feeding considerations.

Additional information was obtained from the ^{48}Ca + ^{238}U experiment. As can be seen in Fig. 11, the four transitions associated with the yrast cascade are present in these data as well. While there is no evidence for the 2630- and 1819-keV levels in the latter data, there is tentative evidence for an additional, weak 1204-keV γ ray on top of the yrast cascade. Just as in ^{58}Cr, the highest yrast transition appears to be Doppler broadened. This observation, together with the weak intensity of the line, justifies its tentative placement. As can be seen in Table III, angular correlation coefficients could be obtained for the strongest yrast transitions in the data from the deep inelastic reaction. Although the error bars on the R_{ac} ratios are rather large because ^{60}Cr is the weakest of the Cr channels observed in the present work, the data are sufficient to propose with some confidence quantum numbers for yrast levels up to $I^\pi = 6^+$.

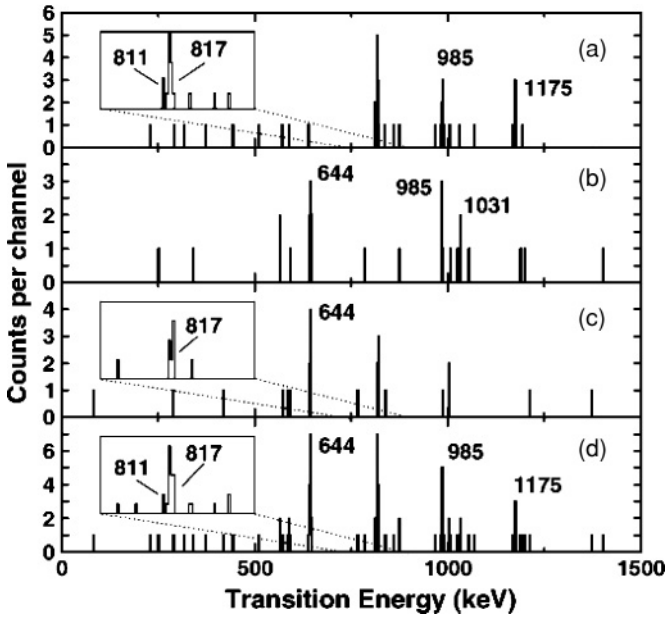

FIG. 9. Coincidence spectra for ^{60}Cr derived from the ^{48}Ca + ^{14}C experiment. The three upper spectra correspond to gates placed on the first three members of the yrast cascade: (a) 644, (b) 817, and (c) 985 keV. A sum of coincidence gates is given in (d). Insets expand the region around the 811- and 817-keV transitions to highlight the relevant coincidence relationships.

IV. DISCUSSION

A. Energy systematics of the 2_1^+ and 4_1^+ states

The excitation energies of the 2_1^+ levels in the Cr nuclei are compared in Fig. 12 (bottom panel) to those in Ti and Fe for all even isotopes with neutron number N between 26 and 36. In addition to the high 2_1^+ energies at $N = 28$ in the three isotopic chains, a peak indicative of the presence of an $N = 32$ subshell closure is also clearly visible in the first two chains, while there is no longer any sign of its presence in the 2_1^+ energy of ^{58}Fe. As stated above, the $N = 32$ shell gap is confirmed further in the Ti and Cr isotopes by the anticorrelation between the high 2_1^+ energies and the low $B(E2; 0^+ \rightarrow 2_1^+)$ transition probabilities [13,20] for this neutron number. Furthermore, as pointed out in Ref. [13], the fact that both the excitation energy and the reduced transition probability observed in ^{54}Ti are comparable to those in ^{50}Ti suggests that the Ti isotope with $N = 32$ is as good a semimagic nucleus as its $N = 28$ counterpart. Clearly,

TABLE III. Levels with spin-parity assignments and γ rays identified in ^{60}Cr, including intensities from both experiments, placements, and relevant ratios from the angular correlation analysis.

E_{level} (keV)	J^π	E_γ (keV)	I_γ (Fusion)	I_γ (Deep inelastic)	R_{ac}	$E_{gate\gamma}$ (keV)
644	2^+	643.9(2)	100(6)	100(5)	1.34(27)	816.8(4)
1461	4^+	816.8(4)	63(10)	86(15)	1.34(27)	643.9(2)
1819	(3, 4)	1175.0(10)	35(10)			
2446	6^+	985.3(2)	49(6)	42(9)		
2630	(5, 6)	811.1(4)	41(8)			
3477	(8^+)	1031.4(3)	43(8)	23(14)	1.44(48)	816.8(4)
4681	(10^+)	1204.0(10)	23(1)	10(5)		

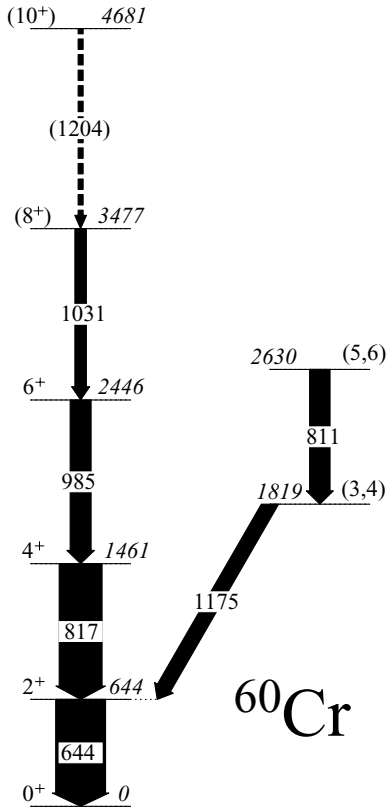

FIG. 10. Proposed level scheme for ^{60}Cr derived from the ^{48}Ca + ^{14}C experiment, in combination with data from the ^{48}Ca + ^{238}U experiment.

the same statement cannot be made for $N = 32$ Cr: the 2_1^+ energy (1007 keV) is markedly lower than the corresponding quantity (1434 keV) in $N = 28$ ^{52}Cr, although the reduced transition probabilities are of the same order in both nuclei [20]. This weakening of the $N = 32$ gap with proton number is understood [12] as being due to the increasing strength of the $\pi 1f_{7/2}$-$\nu 1f_{5/2}$ proton-neutron monopole interaction as protons are added to the $\pi 1f_{7/2}$ shell; this increase results in a gradual lowering in energy of the $\nu 1f_{5/2}$ state to the point

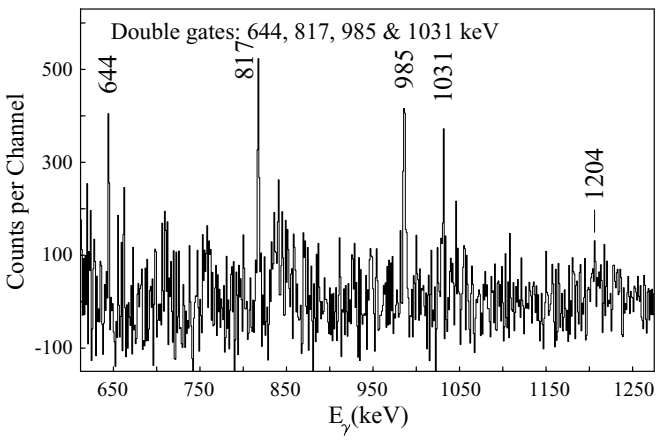

FIG. 11. Example of a sum-coincidence spectrum in ^{60}Cr from the ^{48}Ca + ^{238}U data.

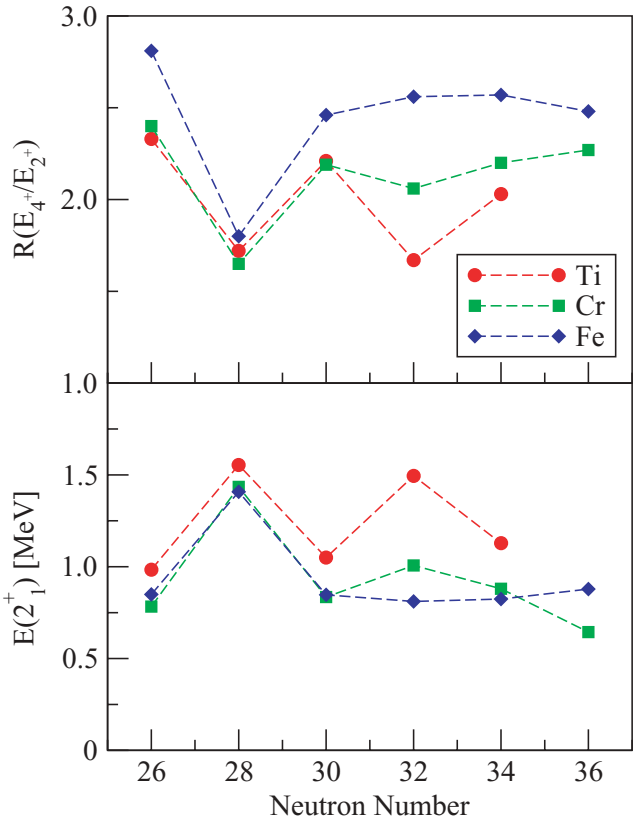

FIG. 12. (Color online) $E(2_1^+)$ and $R(E_{4^+}/E_{2^+})$ systematics for neutron-rich Ti, Cr, and Fe isotopes in the range $26 \leqslant N \leqslant 36$. Data on the Ti isotopes are from Refs. [9,19]; those on the Cr nuclei are from the present work and Ref. [36]. $E(2_1^+)$ values for the Fe isotopes can be found in Ref. [36].

where it impacts the potential presence of a gap above the $\nu 2p_{3/2}$ orbital.

Another noteworthy trend can be observed in the bottom panel of Fig. 12: beyond $N = 32$, the 2_1^+ excitation energies drop steadily in the Cr isotopic chain, in marked contrast with the observations in the Fe isotones. In Ref. [21], it was proposed that this behavior is associated with the onset of deformation with increasing neutron number. Using the empirical expression of Ref. [37] relating the 2_1^+ energy to the quadrupole deformation β_2, Sorlin *et al.* [21] suggested the onset of a sizable deformation in ^{60}Cr, i.e., $\beta_2 \simeq 0.27$, without being able to distinguish between a prolate and an oblate shape on the basis of the available evidence. The present data on ^{60}Cr shed further light on this issue, as illustrated in the top panel of Fig. 12, where the ratios $R(E_{4^+}/E_{2^+})$ of the 4_1^+ to 2_1^+ state energies are given as a function of neutron number. In all the Cr isotopes, the $R(E_{4^+}/E_{2^+})$ values remain well below that characteristic of a deformed rotor (3.33), leading one to question the interpretation in terms of deformation proposed in Ref. [21]. Rather, the present observations concerning transition probabilities and 2_1^+ and 4_1^+ state energies warrant the approach adopted hereafter of first carrying out detailed comparisons of the measured level schemes with shell-model predictions, revisiting the issue of deformation only in the event of poor agreement between data and calculations.

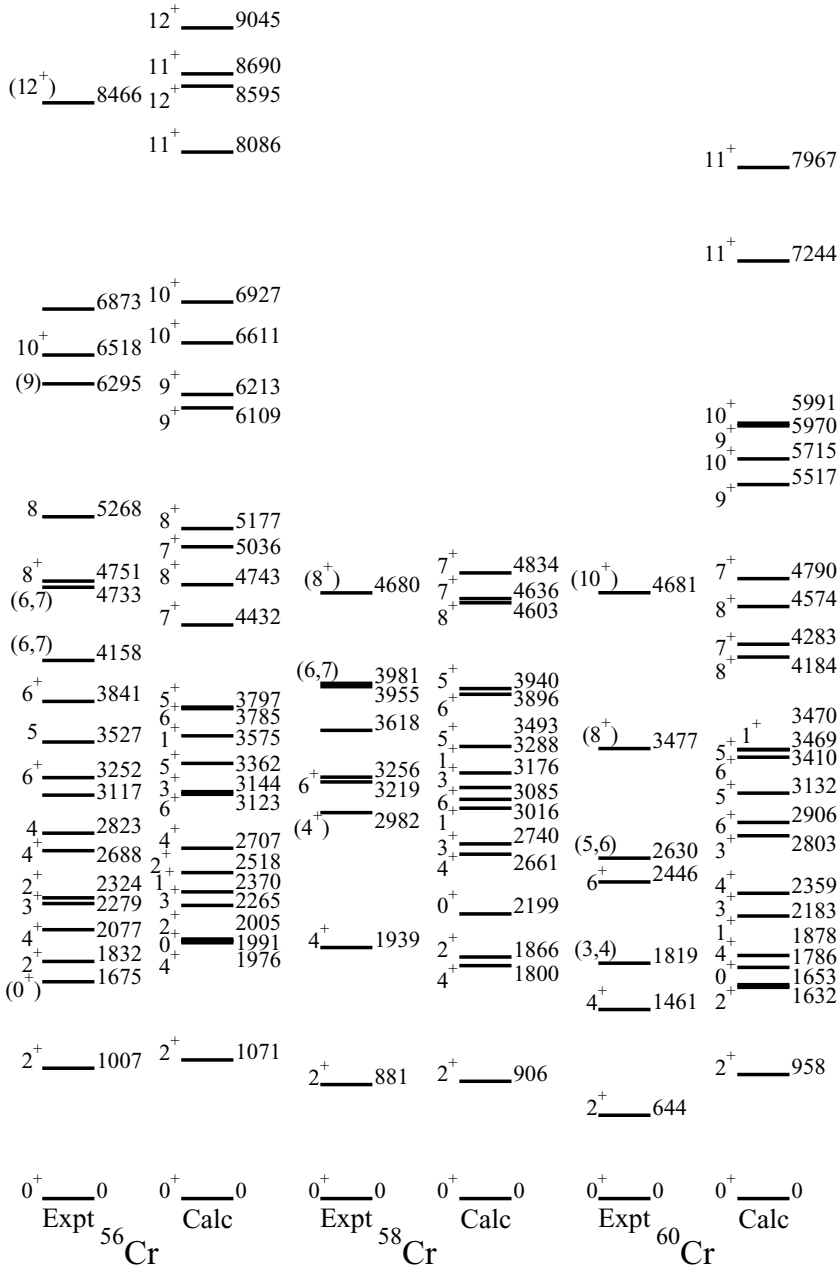

FIG. 13. Comparison between GXPF1A calculations and available data for the positive-parity states in the ^{56,58,60}Cr isotopes. Data are mostly from the present work, but include results from earlier reports [8,11,24,32].

B. Comparison with shell-model calculations

The shell-model calculations presented here were carried out within the full *fp* shell using the GXPF1A Hamiltonian [18]. The latter is a modified version of the GXPF1 effective interaction [12], where five $T = 1$ matrix elements involving mainly the $\nu p_{1/2}$ and $\nu f_{5/2}$ single-particle orbitals were changed. Specifically, more repulsive monopole pairing strengths were adopted for the $p_{1/2}$-$p_{1/2}$ and $p_{1/2}$-$f_{5/2}$ couplings, while the quadrupole-quadrupole interaction between $p_{1/2}$-$f_{5/2}$ orbitals was made more attractive. In addition, a slightly more repulsive $f_{7/2}$-$f_{7/2}$ monopole pairing was adopted as well. The resulting $\nu p_{1/2}$-$\nu f_{5/2}$ gap in the effective single-particle energies becomes narrower for $N \geqslant 34$, and the mixing among the two states becomes larger than was the case with the GXPF1 interaction. This modified interaction has proved to be rather successful in the description of the ^{53,54,56}Ti nuclei [13,19]; it is tested extensively here for the first time in the neutron-rich Cr isotopes. Figure 13 provides a comparison between the data and the results of the calculations for the positive-parity states observed in the three Cr isotopes of interest. The description of the negative-parity levels, which involves the promotion of at least one neutron from the *fp* shell into the $g_{9/2}$ opposite-parity state, is outside the model space and, as a result, has to be considered separately (see below).

As can be seen in Fig. 13, the positive-parity yrast sequence of ^{56}Cr is reproduced satisfactorily by the calculations as the computed 2_1^+, 4_1^+, 6_1^+, 8_1^+, 10_1^+, and 12_1^+ levels lie within 64, 101, 129, 8, 93, and 129 keV of their respective experimental counterparts. While the low-spin yrast states are characterized by wave functions dominated by proton excitations, neutron excitations across the $N = 32$ shell gap certainly play a

significant role at moderate spin ($I \sim 10\hbar$). Hence, the noted agreement between data and theory argues in favor of the validity of the GXPF1A interaction. The model also appears to provide a satisfactory reproduction of most of the other positive-parity levels. For example, the experimental $2_2^+, 3_1^+, 4_2^+$ sequence is reproduced satisfactorily (Fig. 13) with respective energy differences between data and calculations of 173, 14, and 19 keV. Note that the 2_2^+ level is also located close in energy to the 4_1^+ state, as seen experimentally. In the same way, not only is the energy location of the calculated 5_1^+ level close to experiment (165 keV), but also the state is computed to be sandwiched between the first two 6^+ levels, as is experimentally the case with the calculated 6_2^+ state lying within 56 keV of experiment. Because of this success in reproducing the data, it is then tempting to associate measured states for which spin and parity assignments are tentative with some of the computed levels of Fig. 13. For example, the $I = (6, 7)$, 4158-keV state could possibly correspond to the calculated 7_1^+ level at 4432 keV, and the spin 8 level at 5268 keV may well be corresponding to the 5177-keV computed 8^+ state. Only 186 keV would separate the calculated 9_1^+ level from the (9), 6295-keV measured state, but in this case an association with the calculated 9_2^+ state at 6231 keV cannot be ruled out. It is interesting to note that gaps in the calculated and experimental spectra also show some correspondence. For example, the gap in experimental levels at 5268 and 6295 keV is reproduced in the theoretical sequence between the 5177- and 6109-keV states, and gaps in the calculated sequences between 3797 and 4432 keV and between 6927 and 8086 keV seem to have experimental counterparts. All in all, it appears that the positive-parity structure of ^{56}Cr is satisfactorily reproduced, the agreement between data and theory being comparable to that achieved in similar comparisons for the Ti isotopic chain.

Because of the relative paucity of data available for the ^{58}Cr nucleus, comparisons between experiment and calculations are more restricted. Nevertheless, the measured energy sequence of yrast states is reproduced in a satisfactory manner (see Fig. 13). The average energy difference between computed values and the data for the four yrast states is small (94 keV) and of the same order as that observed in ^{56}Cr (76 keV). Thus, the GXPF1A interaction is able to reproduce the drop in 2_1^+ energy between $N = 32$ and $N = 34$ satisfactorily. The agreement with calculations also provides an additional degree of confidence in the tentative assignment of the experimental 4680-keV level as the 8_1^+ yrast state. As Fig. 13 shows, a number of other low-spin excited states are present in the calculated scheme. Some of them most likely correspond to measured levels reported here, but the lack of information, in particular, on spin and parity quantum numbers, makes meaningful comparisons difficult.

As can be seen in Fig. 13, the agreement between the shell-model calculations and the data is strikingly poorer in ^{60}Cr than in the other two even Cr isotopes. Not only is the average energy difference between computed and measured states significantly larger (566 keV), but also a distinct trend is present as the discrepancy increases rapidly with spin. The measured energy difference between calculation and experiment is already 314 keV for the 2_1^+ level, and increases gradually to 1034 keV by the time the 10_1^+ state is reached. These observations are valid not only for the yrast states, but also for the two additional levels that have been observed, irrespective of the uncertainties associated with their quantum numbers. For example, the discrepancy between experiment and theory is 364 or 540 keV for the 1819-keV level, depending on whether a spin value of 3 or 4 is adopted. Thus, it appears that the experimental ^{60}Cr level structure is compressed with respect to the GXPF1A prediction.

The findings derived here about (i) the adequacy of the shell-model description with the GXPF1A Hamiltonian for ^{56,58}Cr and (ii) its failure to reproduce the structure of ^{60}Cr also apply to the odd neighboring Cr nuclei, as illustrated in Fig. 14. Indeed, a satisfactory description of the negative-parity states in ^{55,57}Cr is achieved with the same interaction. For example, the yrast sequence in $N = 31$, ^{55}Cr, from the $1/2^-$ ground state to the level with the highest spin $(17/2^-)$, is reproduced with an average energy difference between experiment and theory of 76 keV, which is similar to that reported above for ^{56}Cr. Admittedly, the present experimental knowledge of negative-parity states in ^{57}Cr is more limited. Nevertheless, the measured and calculated level sequences agree within an average energy of 132 keV, and the overall level sequence is well reproduced, even though the calculations invert the first excited state and the ground state. Finally, despite uncertainties regarding spin and parity quantum numbers, the experimental sequence in ^{59}Cr is visibly compressed with respect to the calculations. For example, the first excited $(3/2^-)$ state is predicted to lie 339 keV higher than seen in the data, and the discrepancy increases further to 453, 495, and 1273 keV for the $(5/2^-)$, $(7/2^-)$, and $(11/2^-)$ yrast states.

The inadequacy of the GXPF1A interaction for the description of Cr isotopes beyond $N = 34$ can possibly be viewed as an indication that the *fp* shell-model space becomes too restrictive as one gets closer to the weak $N = 40$ subshell closure. The compression seen in the experimental levels compared to the calculated ones may be due to the influence of configurations originating above the gap. If these configurations were included in the calculation, additional mixing would occur, resulting in a compression of the computed yrast sequence and yielding better agreement with experiment. A natural candidate for inclusion in an expanded description appears to be the $\nu g_{9/2}$ orbital. As discussed hereafter, the present data as well as those on the odd ^{55,57,59}Cr nuclei provide strong experimental indications of the importance of this intruder orbital and of the need to take it into account in order to achieve a satisfactory description.

C. Role of the $g_{9/2}$ neutron orbital

The impact of the $\nu g_{9/2}$ orbital on the level structure of neutron-rich Cr isotopes was highlighted recently by Deacon *et al.* [22] in the case of the odd ^{55,57,59}Cr nuclei. As stated in the Introduction, $9/2^+$ levels associated with this orbital have been seen in the three odd isotopes: their excitation energy drops from 2087 keV at $N = 31$ to 1507 at $N = 33$ and to only 503 at $N = 35$. Furthermore, cascades of $E2$ transitions were observed in the lightest two isotopes which

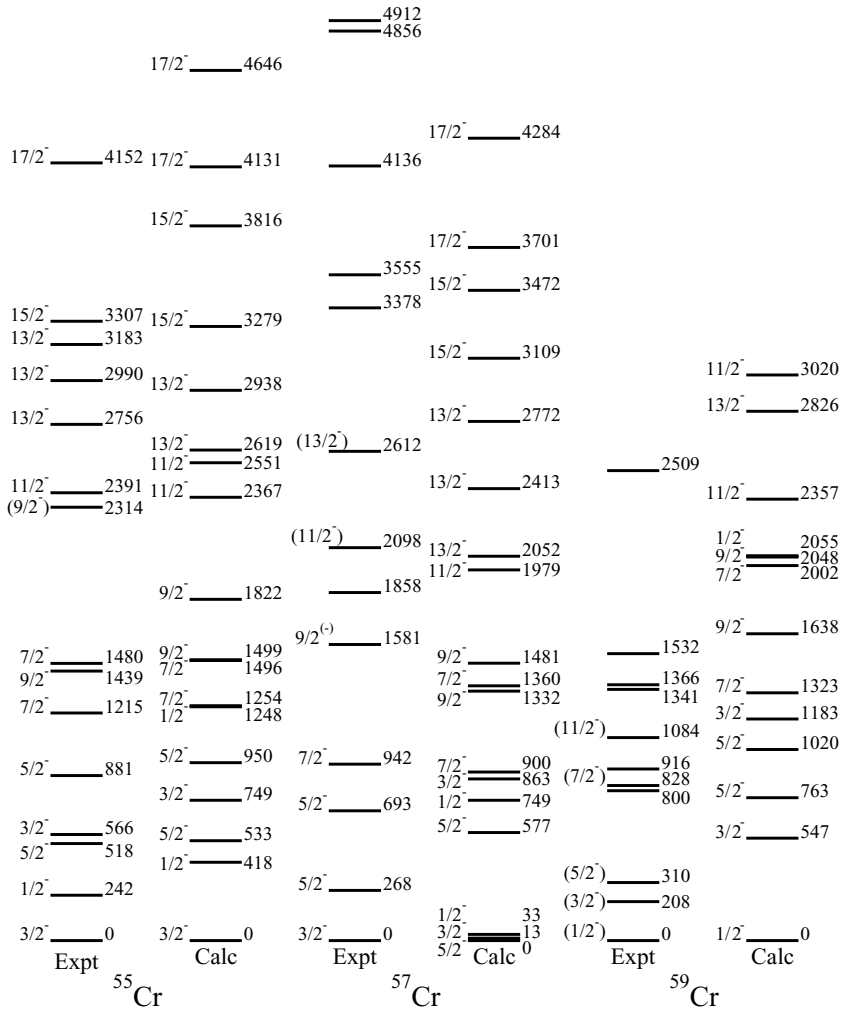

FIG. 14. Comparison between GXPF1A calculations and available data [11,22,23] for the negative-parity states in the ^{55,57,59}Cr isotopes.

were associated in Refs. [11,22] with decoupled rotational bands. In ^{57}Cr in particular, the rotational band was traced up to the $(37/2^+)$ level which was proposed to be associated with the terminating state of the $\pi f_{7/2}^4 \nu g_{9/2}(f_{5/2}p_{3/2}p_{1/2})^4$ configuration. Total Routhian surface (TRS) calculations [38] with this configuration reproduce the experimental observations when the $g_{9/2}$ neutron occupies the $1/2^+[440]$ orbital with an associated prolate shape. These calculations reproduce the ^{55}Cr data of Ref. [11] as well. The situation is markedly different in ^{59}Cr. Only in this case is the $9/2^+$ level isomeric, implying that it must be interpreted as a band head, and there is thus far no evidence for a rotational cascade [23]. These observations have led to an interpretation in terms of a band head dominated by the $9/2^+[404]$ configuration which is also of $g_{9/2}$ parentage, but it is favored only at oblate deformation [22].

Figure 15 (left panel) illustrates the striking similarity between the negative-parity, spin 7 to 17, sequence of ^{56}Cr (Fig. 1) and the two decoupled bands in the odd neighbors. The aligned angular momentum I_x experiences a similar increase with rotational frequency in all three bands, except perhaps at the highest spins where the beginning of a backbend is, tentatively, present in ^{57}Cr. As a result of this observation, TRS calculations of the same type as those of Refs. [11,22] were carried out in order to track both the ground-state configuration and a negative-parity, two-quasineutron configuration similar to those considered in the odd neighbors, i.e., with one particle

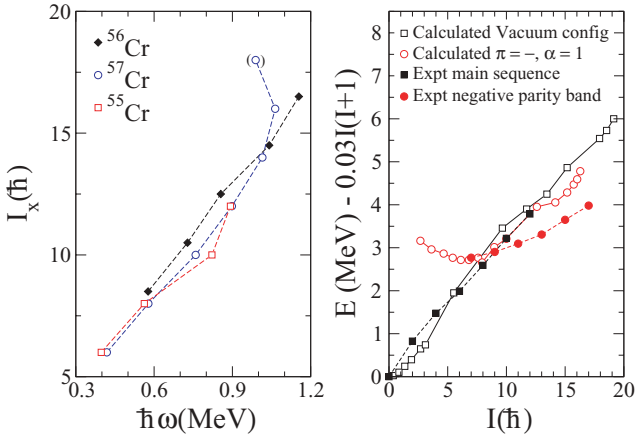

FIG. 15. (Color online) Experimental angular momentum alignments along the rotation axis, I_x, as a function of rotational frequency for the bands associated with the $g_{9/2}$ orbital in $^{55-57}$Cr (left panel). Excitation energy (minus a reference) vs spin from experimental data and TRS calculations in ^{56}Cr (right panel).

occupying the same prolate-driving $1/2^+[440]$ orbital of $g_{9/2}$ parentage and the other the $f_{5/2}$ state, emptying the $p_{3/2}$ and/or $p_{1/2}$ states correspondingly. A comparison between the data and the results of the calculation is provided in the right panel of Fig. 15 in the form of an excitation energy (minus a reference) vs spin plot. Since the $1/2^+[440]$ orbital is characterized by a large decoupling parameter, only the favored ($\alpha = 1$) signature would be expected to be observed experimentally; as a result, it is the only one considered in Fig. 15. As in the earlier work, the Woods-Saxon parameters were those of the so-called "universal set" of Ref. [39]. The ground-state trajectory in Fig. 15 is associated with a prolate shape with deformation parameters $\beta_2 = 0.18$, $\gamma \sim 0^\circ$; while the negative-parity, two-quasineutron excitation is characterized by a somewhat larger prolate deformation of $\beta_2 = 0.24$, $\gamma \sim 4^\circ$ associated with the deformation-driving effects of the $g_{9/2}$ state. As can be seen from the figure, the calculations predict rather well the trajectory of the ground-state band for spins $I > 6\hbar$. The spin range in which the crossing with the negative-parity structure occurs is also accounted for, even though the slope of the theoretical curve associated with this excitation is somewhat steeper than that seen in the experiment. Considering the fact that the calculations are based on a parameter set that was deduced from data on nuclei near stability and has not been adjusted or tested on neutron-rich nuclei, the agreement can be viewed as satisfactory.

The TRS calculations were extended further to the ^{58}Cr and ^{60}Cr isotopes in order to investigate these shape-driving effects with increasing mass. Ground-state deformation surfaces for these two nuclei are compared with that of ^{56}Cr in Fig. 16. It is apparent that as the mass increases, the potential is becoming progressively softer (in the γ degree of freedom) and a well defined, deep minimum is no longer present in deformation space. This increasing softness is certainly consistent with the drop in the 2_1^+ state energies and with the values of the $R(E_{4^+}/E_{2^+})$ ratios noted above. This conclusion from the calculations can then be combined with the present understanding of the ^{59}Cr data [23] which also supports the picture of a ground state that is either spherical or, preferably, associated with a small oblate deformation, driven by the $9/2^+[404]$ Nilsson configuration. If a soft, spherical or slightly oblate minimum indeed defines the shape of ^{58}Cr, it is likely that any negative-parity configuration involving a $g_{9/2}$ neutron

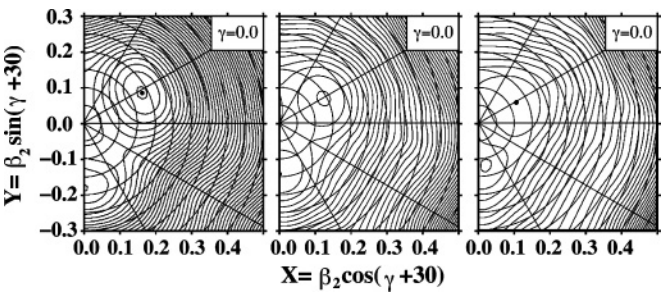

FIG. 16. Ground-state potential energy surfaces for ^{56,58,60}Cr (left to right panels, respectively) from the TRS calculations described in the text. Contours are shown at 200-keV intervals; location of the absolute minimum is indicated by a dot in each panel.

will be associated with the high-Ω Nilsson orbital and will translate into the presence of a strongly-coupled band structure in the level scheme. The present data (Fig. 5) are insufficient to draw definite conclusions, although the tentative negative-parity sequence of alternating odd and even spins, starting with the 3311-keV, $5^{(-)}$ level, is suggestive of such a band structure. More extensive data for ^{60}Cr would also be needed to place this interpretation on a stronger footing. While additional experimental work would clearly help, there are also issues on the theoretical side requiring further attention. These issues were identified in Ref. [22] for the odd neutron-rich Cr isotopes and are echoed here for the even nuclei. Systems exhibiting significant softness and wide, poorly defined minima are most affected by effects neglected in the current models such as the coupling of specific shape-driving configurations to a soft core, for example. In addition, the usage of the universal parameter set for these nuclei needs to be validated, or, alternatively, a modified set for the description of neutron-rich nuclei needs to be developed.

Even if a complete, quantitative picture is not yet emerging from the present discussion, it is clear that the $g_{9/2}$ orbital cannot be ignored in the description of $N \geqslant 34$ Cr isotopes and that shell-model calculations in a full *fpg* space are highly desirable. Unfortunately, an effective interaction for such a space is currently lacking, although first preliminary attempts at developing it are underway. Preliminary results of this theoretical work indicate that a noticeable compression of the calculated yrast level spacings occurs for the case of ^{60}Cr [40], in line with the observations reported above.

V. CONCLUSIONS

The even-even, neutron-rich ^{56,58,60}Cr isotopes were investigated at Gammasphere using several techniques. Specifically, deep inelastic reactions of ^{48}Ca beams on thick ^{208}Pb and ^{238}U targets, as well as a fusion-evaporation reaction with the same beam, but a ^{14}C radioactive target were used to obtain the data sets from which new structural information was derived.

In ^{56}Cr and ^{58}Cr, the positive-parity states were described in a satisfactory manner over the entire spin and excitation energy range by shell-model calculations using the recently developed GXPF1A interaction. Thus, the calculations account for a subshell closure at neutron number $N = 32$ and its absence at $N = 34$. However, the experimental level structure of $N = 36$, ^{60}Cr is more compressed than that calculated; i.e., beyond $N = 34$, the *fp* model space appears to be too restrictive to account for the observations. In this way, the data on these even Cr nuclei confirm conclusions reached earlier [22] based on data on the $N = 31, 33, 35$ isotopes, where the low-spin levels in the first two odd Cr nuclei were satisfactorily described by the shell-model calculations while those in the heaviest one were not.

The close similarity between the odd and even Cr isotopes extends further to the states in which the intruder $g_{9/2}$ orbital plays a role. Its presence manifests itself in $^{55-57}$Cr through the appearance at moderate spin and excitation energy of rotational bands exhibiting strikingly similar alignment patterns in all three isotopes. In this respect, too, the two heaviest Cr nuclei

appear to be different: there is no sign of a collective excitation in either the odd or the even nucleus. Furthermore, a low-lying isomer associated with the $g_{9/2}$ state is present in ^{59}Cr.

The picture that emerges from these comparisons is one in which the intruder, shape-driving $g_{9/2}$ orbital needs to be taken into account to achieve a satisfactory overall description. In the lightest Cr nuclei under study here, excitations involving this state appear in the experimental spectrum at sufficiently high excitation energy and angular momentum that they do not seem to disturb significantly the single-particle states associated with the *fp* space. The impact of the $g_{9/2}$ orbital is nevertheless significant as the presence of rotational bands indicates that the nuclear shape becomes prolate once this excitation is involved. Total Routhian surface calculations account for the observations in $^{55\text{-}57}$Cr in a satisfactory manner. As the neutron number increases, the $g_{9/2}$ state continues to come closer to the Fermi surface, and there are indications that the structure of ^{59}Cr is best explained in terms of excitations associated with an oblate shape with modest deformation. The TRS calculations with existing parametrizations encounter difficulties in reproducing the observations in detail, although they indicate that the nuclear potential becomes rather soft and that a well-defined shape is absent in $^{58-60}$Cr. Shell-model calculations in the enlarged *fpg* space as well as TRS calculations with parameters suitable for neutron-rich nuclei of the region are badly needed to investigate the issues further.

In any event, it appears that the shape-driving effects observed in the Cr isotopes investigated here are less pronounced than those seen in $N = Z$ nuclei with mass $A \sim 60$–70, where both protons *and* neutrons fill the same orbitals as neutrons do here. As discussed in Ref. [22], the nuclei of the two regions have common structural features, but stronger cooperative shape polarization effects are present when both types of nucleons share orbitals with the same shape-driving character.

ACKNOWLEDGMENTS

The authors thank M. Freer for the loan of the ^{14}C target, the operating staff of ATLAS for the quality of the ^{48}Ca beams, J. P. Greene for target fabrication, and J. Rohrer for the technical support. This work was supported by the U.S. Department of Energy, Office of Nuclear Physics, under Contract No. E-AC02-06CH11357, by the U.K. Engineering and Physical Sciences Research Council, by U.S. National Science Foundation Grants No. PHY-01-01253 and PHY-0456463, and by Polish Scientific Committee Grant No. 2PO3B-074-18.

[1] B. A. Brown, Prog. Part. Nucl. Phys. **47**, 517 (2001).
[2] R. V. F. Janssens, Nature (London) **435**, 897 (2005).
[3] T. Motobayashi *et al*., Phys. Lett. **B346**, 9 (1995).
[4] R. Ibbotson *et al*., Phys. Rev. Lett. **80**, 2081 (1998).
[5] B. V. Pritychenko, T. Glasmacher, B. Brown, P. D. Cottle, R. W. Ibbotson, K. W. Kemper, L. A. Riley, and H. Scheit, Phys. Rev. C **63**, 011305(R) (2001).
[6] E. K. Warburton, J. A. Becker, and B. A. Brown, Phys. Rev. C **41**, 1147 (1990).
[7] Y. Utsuno, T. Otsuka, T. Mizusaki, and M. Honma, Phys. Rev. C **64**, 011301(R) (2001).
[8] J. I. Prisciandaro *et al*., Phys. Lett. **B510**, 17 (2001).
[9] R. V. F. Janssens *et al*., Phys. Lett. **B546**, 55 (2002).
[10] A. Huck, G. Klotz, A. Knipper, C. Miehé, C. Richard-Serre, G. Walter, A. Poves, H. L. Ravn, and G. Marguier, Phys. Rev. C **31**, 2226 (1985).
[11] D. E. Appelbe *et al*., Phys. Rev. C **67**, 034309 (2003).
[12] M. Honma, T. Otsuka, B. A. Brown, and T. Mizusaki, Phys. Rev. C **65**, 061301(R) (2002).
[13] D. C. Dinca *et al*., Phys. Rev. C **71**, 041302(R) (2005).
[14] A. Gade *et al*., Phys. Rev. C **74**, 021302(R) (2006).
[15] B. Fornal *et al*., Phys. Rev. C **70**, 064304 (2004).
[16] S. N. Liddick *et al*., Phys. Rev. Lett. **92**, 072502 (2004).
[17] S. N. Liddick *et al*., Phys. Rev. C **70**, 064303 (2004).
[18] M. Honma, Eur. Phys. J. A **25**, 499 (2005).
[19] B. Fornal *et al*., Phys. Rev. C **72**, 044315 (2005).
[20] A. Bürger *et al*., Phys. Lett. **B622**, 29 (2005).
[21] O. Sorlin *et al*., Eur. Phys. J. A **16**, 55 (2003).
[22] A. N. Deacon *et al*., Phys. Lett. **B622**, 151 (2005).
[23] S. J. Freeman *et al*., Phys. Rev. C **69**, 064301 (2004).
[24] P. F. Mantica *et al*., Phys. Rev. C **67**, 014311 (2003).
[25] N. Mărginean *et al*., Phys. Lett. **B633**, 696 (2006).
[26] S. J. Freeman *et al*., J. Phys. G: Nucl. Part. Phys. **31**, S1465 (2005).
[27] R. Broda, J. Phys. G: Nucl. Part. Phys. **32**, R151 (2006).
[28] B. Fornal *et al*., Acta Phys. Pol. B **26**, 357 (1995).
[29] W. Królas, R. Broda, B. Fornal, T. Pawlat, H. Grawe, K. Maier, M. Schramm, and R. Schubart, Nucl. Phys. **A724**, 289 (2003).
[30] I. Y. Lee, Nucl. Phys. **A520**, 641c (1990).
[31] C. N. Davids, Nucl. Instrum. Methods B **70**, 358 (1992).
[32] O. Sorlin *et al*., Nucl. Phys. **A632**, 205 (1998).
[33] A. M. Nathan, J. W. Olness, E. K. Warburton, and J. B. McGrory, Phys. Rev. C **16**, 192 (1977).
[34] C. W. Beausang *et al*., Nucl. Instrum. Methods Phys. Res. A **452**, 431 (2000).
[35] A. N. Deacon, Ph.D. thesis, University of Manchester, 2006.
[36] R. Firestone, *Table of Isotopes,* 8th ed. (Wiley, New York, 1996), Vol. 1.
[37] S. Raman, C. W. Nestor Jr., S. Kahane, and K. H. Bhatt, Phys. Rev. C **43**, 556 (1991).
[38] W. Nazarewicz and A. Wyss, Nucl. Phys. **A503**, 285 (1989).
[39] W. Nazarewicz, J. Dudek, R. Bengtsson, and I. Ragnarsson, Nucl. Phys. **A435**, 397 (1985).
[40] M. Honma (to be published).